THE NUCLEAR LIQUID-GAS PHASE TRANSITION: PRESENT STATUS AND FUTURE PERSPECTIVES

J. POCHODZALLA

Max-Planck Institut für Kernphysik,Saupfercheckweg 1,
69177 Heidelberg, Germany

G. IMME', V. MADDALENA, C. NOCIFORO, G. RACITI, G. RICCOBENE,
F.P. ROMANO, A. SAIJA, C. SFIENTI, G. VERDE

Dipartimento di Fisica - Universitá di Catania and I.N.F.N.- Laboratorio Nazionale del Sud and Sezione di Catania
I-95123 Catania, Italy

M. BEGEMANN-BLAICH, S. FRITZ, C. GROß , U. KLEINEVOß ,
V. LINDENSTRUTH, U. LYNEN, M. MAHI, W.F.J. MÜLLER, B. OCKER,
T. ODEH, T. RUBEHN, H. SANN, M. SCHNITTKER, C. SCHWARZ,
V. SERFLING, W. TRAUTMANN, A. WÖRNER, E. ZUDE

Gesellschaft für Schwerionenforschung mbH,
D-64220 Darmstadt, Germany

T. MÖHLENKAMP, W. SEIDEL

Forschungszentrum Rossendorf,
D-01314 Dresden, Germany

W.D. KUNZE, A. SCHÜTTAUF

Institut für Kernphysik,Universität Frankfurt,
D-60486 Frankfurt, Germany

G.J. KUNDE, S. GAFF, H. XI

Department of Physics and Astronomy and National Superconducting Cyclotron Laboratory, Michigan State University,
East Lansing, MI 48824, USA

R. BASSINI, I.IORI, A. MORONI, F. PETRUZZELLI

I.N.F.N. Sezione di Milano and Department of Physics - University of Milano,
I-20133 Milano, Italy

A. TRZCINSKI, B. ZWIEGLINSKI

Soltan Institute for Nuclear Studies,
00-681 Warsaw, Hoza 69, Poland

More than two decades ago, the van der Waals behavior of the nucleon - nucleon force inspired the idea of a liquid-gas phase transition in nuclear matter. Heavy-ion reactions at relativistic energies offer the unique possibility for studying this phase transition in a finite, hadronic system. A general overview of this subject is given emphasizing the most recent results on nuclear calorimetry.

1 The Essence of Nuclei

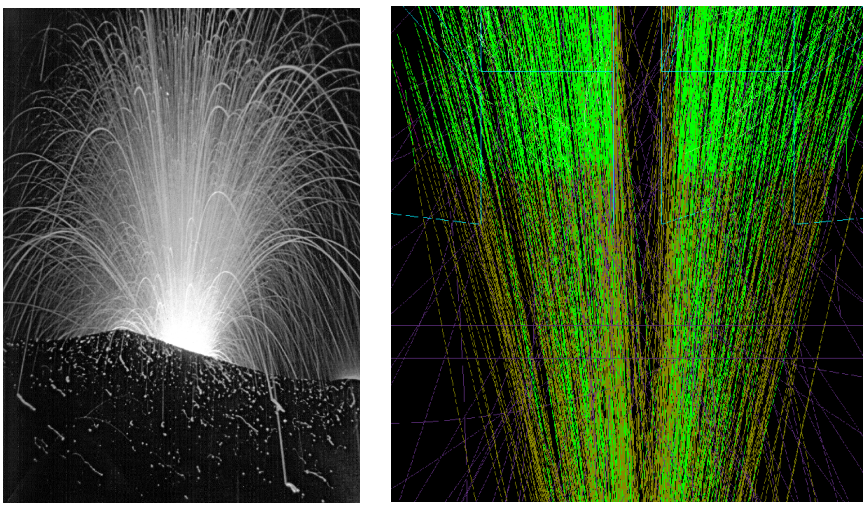

Figure 1: Left: Empedocles' view of the world. Right: Expanded view of Pb-Pb collisions at 160 GeV/u recorded by the NA49 TPC's at the CERN/SPS.

Of what are nuclei made? Let us approach this question by asking – even more general – of what is the *world* made? If we would have asked Empedocles of Acragas – the Greek philosopher, statesman and poet who was born here in Sicily nearly 2500 years ago – he would have answered [1]: The world is composed of four primal elements *earth, water, air* and *fire*. I am sure that the development of these ideas was inspired by the extraordinary surroundings of his homeland where everybody could [2] – and still can (Fig.1, left) – directly experience the forces of these elements.

Today, of course, we would respond to this question quite differently: we and the world around us consist out of more than 100 elements, some of which give only a short interlude after their production. These atoms themselves are made of electrons and nuclei, the latter being clusters of protons and neutrons. Those are again only combinations of gluons and quarks and today even quarks can no longer be safely considered as elementary particles.

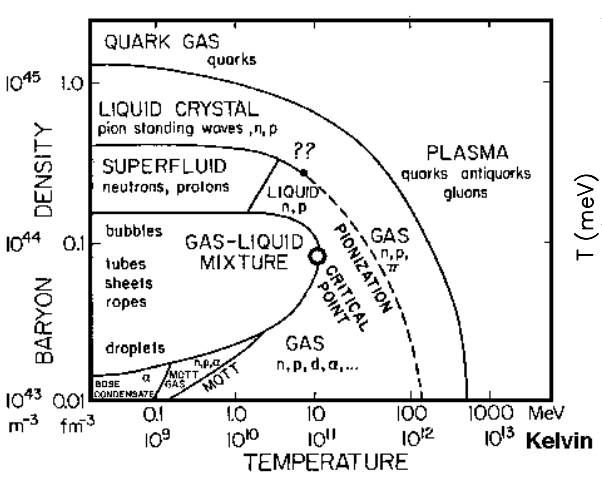

Figure 2: Conceivable landscape of hadronic and nuclear phases [5]. While most regions of this diagram are *terra incognita*, both, the liquid and the gaseous phase of nuclear systems are known to exist.

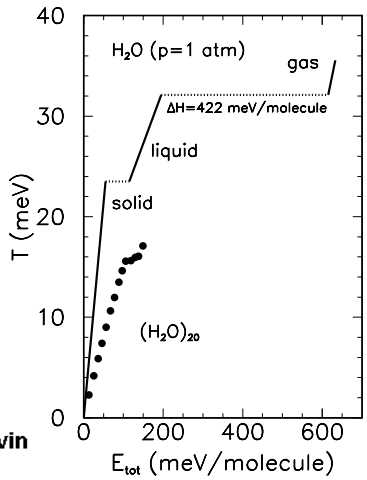

Figure 3: Caloric curve of bulk water at atmospheric pressure (line) and of a water clusters consisting of 20 H_2O molecules predicted [36] by molecular dynamics calculations (dots).

Thus, this microscopic view of the world – an impressive illustration of the technical progress made with respect to our 'resolving power' over the last years is shown in the right part of Fig.1 – seems to bring us close to the final answer of our primary question. But will it provide us with a full answer? Is Empedocles' antique view of the world already obsolescent? Probably not, if we look at the physical world from a more naive point of view. For example, a glass of liquid water cooled below 0^oC will freeze to ice showing the solid character of earth. Water heated above 100^oC will build an airy gas. Finally, at high temperatures atoms disintegrate into a plasma of electrons and ions which – loosely speaking –may be considered as the analog to fire. In that sense the four roots *earth, water, air* and *fire* being representative for *solids, liquids, gases* and *plasmas* are omnipresent in our everyday life. Today these states of matter are called *phases*.

1.1 The Nuclear Paradigm

The prospect of creating a phase of matter resembling that of the pre-hadronic phase of the early universe or of the core of today's neutron stars [3] is one of

the prime motivations to study relativistic heavy ion collisions. Unquestionable, the transition to the quark-gluon plasma represents the most spectacular example of a phase transition in nuclear matter. The complex structure of the hadronic components and the many facets of their interaction [4], however, offer the opportunity to observe in addition several other, exciting nuclear state transitions (Fig. 2, from ref. [5]). Already two decades ago, the van der Waals behavior of the nucleon - nucleon force inspired the idea of a liquid-gas phase transition in nuclear matter [6–8]. What makes this nuclear liquid gas phase transition stand out from all other conceivable nuclear phase transitions though, is the fact that both phases, cold nuclear Fermi liquids on the one hand and a nuclear gas consisting of free nucleons and a few light clusters on the other hand, are known to exist in nature, and, what may perhaps be even more important, that both are experimentally accessible. This unique feature makes the nuclear liquid-gas phase transition an ideal and relevant test case for our ability to identify and quantify a phase transition in a finite hadronic system.

The first observation of a self-similar power law for the fragment mass distribution in proton induced reactions was interpreted as an indication for a critical phenomenon [9]. Despite enormous effort during the last decade [10–12], the attempts to deduce critical parameters [8] and critical point exponents [13–15] remained elusive [16–19]. Searching for signals of a nuclear phase transition, we have to cope with several complications: Excited nuclei are transient systems which have to be generated in nuclear collisions. We are, therefore, facing the difficulty to produce isolated nuclear systems which have reached the highest possible degree of equilibration. Nuclei are composed of a limited number of constituents. In a finite system, fluctuations are limited. Singularities of phase transitions get, therefore, rounded and shifted with respect to their bulk values [20,21]. In addition, the long-range Coulomb-repulsion between the constituent protons introduces additional instabilities [22,23] which may lead to a further downward shift of the apparent 'critical' temperature [24–26]. Since no external fields (e.g. pressure) can be applied to excited nuclei in the laboratory [27,28], they may expand prior to their disassembly [29–34]. Eventually, these expanded systems may aggregate into clusters.

Although all these difficulties are inherent in nuclear systems, they do also apply to other fields where finite systems are involved [35]. This is illustrated in Fig. 3 for the case of water. The solid line shows the well-known caloric curve of water at normal pressure of 1 atmosphere. Comparing this paradigm of first-order phase transitions to the predicted [36] caloric curve of a finite H_2O cluster (dots in Fig. 3) we still recognize the characteristic 'plateau' signaling the solid-to-liquid transition. However, the transition temperature is reduced

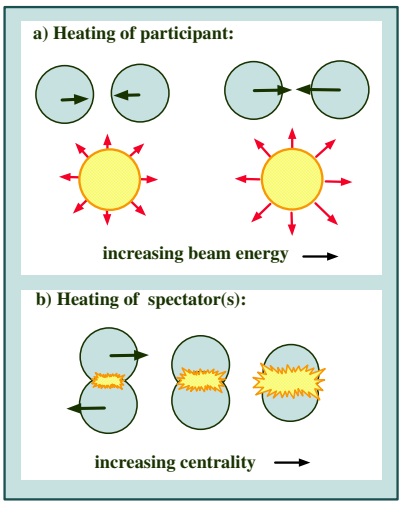

Figure 4: Pictorial view of the two different ways to produce boiling nuclei.

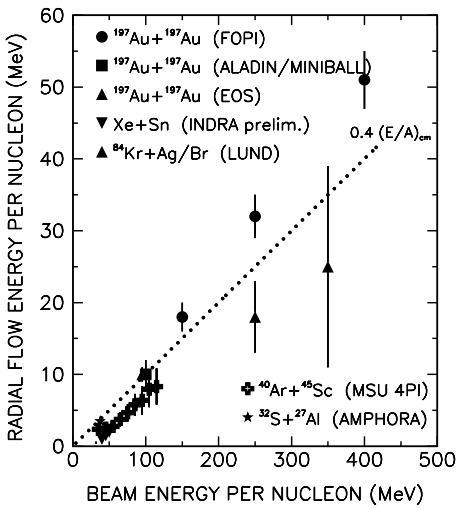

Figure 5: Systematics of radial flow energies in (nearly) symmetric nucleus-nucleus collisions as a function of the beam energy per nucleon.

and distributed over a finite temperature range. Nevertheless, this example illustrates that phase transitions of rather small clusters (∼10 constituents) are still well defined, distinguishable[21,36–38] and – in case of atomic clusters[39] – even detectable, thus nourishing the hope that nuclear systems produced in energetic heavy ion collisions may also exhibit sufficiently clear signatures of a phase transition.

2 The Making of Boiling Nuclei

Heavy-ion reactions at relativistic bombarding energies offer a wide range of possibilities to produce nuclear systems with excitation energies around the nuclear binding energy (Fig. 4).

In head on collisions between equally heavy nuclei the excitation is determined by the incident beam energy. The clear advantage of this method is that, for a given target-beam combination, systems with nearly constant mass number can be produced. However, a significant fraction of the energy is not converted into heat but in collective explosive motion, thus introducing an additional degree of freedom.

Spectator nuclei produced in more peripheral collisions do not show this

collective motion in the *initial* stage, though some radial flow may arise during the thermally driven expansion [34] and may contribute to the kinetic energies of the fragments [60] (see also chapter 2.3). As it is illustrated in the bottom part of Fig. 4, in these collisions the heating is controlled by the size of the fireball and, hence, by the impact parameter.

2.1 The Little Big-Bang

The largest fragment multiplicities measured so far were observed in central ^{197}Au on ^{197}Au collisions at a bombarding energy of 100 MeV per nucleon [40]. In these collisions the system of nearly 400 nucleons disintegrates completely into nuclear fragments and light particles. An analysis of the kinetic energy spectra in these reactions has revealed a considerable collective outward motion superimposed on the random motion of the constituents at the breakup stage (radial flow) which represents a significant fraction of the energy available in the center-of-mass frame [41,42]. This feature prevails, with monotonously increasing flow values, over the range of bombarding energies up to 1000 MeV per nucleon [41–47] (Fig.5).

It demonstrates the strong dynamical coupling between entrance and exit channels in central collisions of heavy systems. Indeed, the process of fragment formation is found to be sensitive to the flow dynamics. The measured relative element yields are systematically correlated with the magnitude of the observed radial flow [44,48]. Within a coalescence picture, the suppression of heavier fragments for larger flow values may be caused by the reduction of the density in momentum space associated with the collective expansion [48].

2.2 The Universality of Spectator Decay

While this interplay of dynamical and statistical effects in central collisions is currently a matter of high interest [49] and remains a challenging subject for future studies, we will now turn to multifragmentation processes in more peripheral nucleus-nucleus collisions at high energies. In contrast to central collisions, no apparent dependence on the entrance channel is observed in the decay of spectator nuclei. The decay patterns were found to be mainly governed by the energy transfer to the spectator, as evident from the Z_{bound} scaling of the fragment charges and their correlations [50,51]. The quantity Z_{bound} is defined as the sum of the charges of all product nuclei with $Z \geq 2$ and is related to the energy deposition. When plotted as a function of this quantity the fragment multiplicities and correlations exhibit a universal behaviour. It was first observed as an invariance with respect to the chosen target in the decays of ^{197}Au projectiles at 600 MeV per nucleon [50,52].

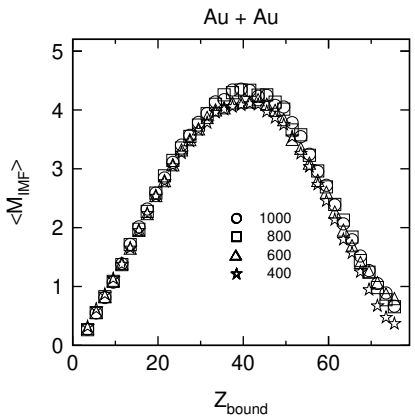

Figure 6: Mean intermediate mass fragment (IMF, $3 \leq Z \leq 30$) multiplicity $\langle M_{IMF} \rangle$ as a function of Z_{bound} for the reaction of ^{197}Au on ^{197}Au at E/A = 400, 600, 800, and 1000 MeV (from ref. [53]).

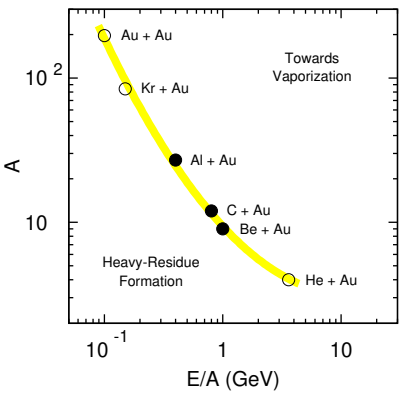

Figure 7: Location of reactions for which maximum fragment production has been observed in the most violent collisions in a two-dimensional map of projectile mass versus bombarding energy. Full points denote reactions studied by the ALADIN collaboration in reverse kinematics, open symbols refer to work reported in [40,55,56] (from ref. [53]).

In Fig. 6 the mean number of intermediate mass fragments is shown as a function of Z_{bound} for the reaction of ^{197}Au on ^{197}Au at four bombarding energies. The correlation between the two quantities is seen to be independent of the projectile energy within the experimental accuracy. The maximum mean multiplicity of 4 to 4.5 fragments is reached at $Z_{bound} \approx 40$.

The observed invariance with respect to the entrance channel is not restricted to the multiplicity of intermediate-mass fragments but appears to be a very general feature of the relative asymmetries and other correlations between the abundance and the atomic numbers of the fragmentation products [51,53]. Scaled with the size of the decaying system, the multiplicity of produced IMF's seems even to be a universal function which is independent of the mass of the decaying system [53,54].

The maximum of the IMF production marks the borderline between the regime of residue formation and vaporization. Our data for collisions with rather light targets such as beryllium or carbon indicate that, in these cases, beam energies considerably above 400 MeV per nucleon are required in order to reach the maximum IMF production as a dominant process. Combining the

ALADIN results with work reported by other groups [40,55,56] we can draw the borderline between the 'liquid-like' and the 'gaseous' regime as shown in Fig. 7 as a function of the target mass.

2.3 Energy Deposition

The invariant features of the spectator multi-fragment decay are consistent with equilibration of the excited systems prior to their decay which justifies interpretations in statistical or thermodynamical terms. The necessary baseline for such considerations is a knowledge of the energy transfer to the excited primary nuclear system. On the other hand, the transient nature of finite nuclear systems makes it difficult to arrive at a unique definition of the decaying system and its associated excitation energy. Depending on the observables we consider, it may characterize different stages of the reaction. In turn, a detailed understanding of the different type of excitation energies might help to understand the temporal evolution of the system.

The procedure used to determine the initial mass and excitation energy of the spectators prior to their decay is very similar to that proposed by Campi *et al.* [57]. The basic idea is to determine the invariant mass (and hence the excitation energy with respect to a nucleus in it's groundstate) as well as the total charge and mass numbers of the system by summing up all masses and kinetic energies.

The results for the mass A_0 and the specific excitation energy E_0/A_0 are given in Fig. 8. The data points represent the results for individual bins in the Z_{max}-versus-Z_{bound} event representation. The mass A_0 decreases with decreasing Z_{bound} but is, apparently, independent of Z_{max}. The smallest mean spectator mass in the bin of $Z_{bound} \leq 10$ is $\langle A_0 \rangle \approx 50$. Reconstructing the impact parameter from the quantity Z_{bound}, one finds that $\langle A_0 \rangle$ is remarkably well described by the simple participant-spectator geometry (see horizontal bars in Fig. 8).

The excitation energy E_0 appears to be a function of both Z_{bound} and Z_{max}; the higher values correspond to the smaller Z_{max} values, i.e. to more complete disintegration of a system of given mass. The maximum number of fragments, observed at $Z_{bound} \approx 40$, is associated with initial excitation energies of $\langle E_0 \rangle / \langle A_0 \rangle \approx 8$ MeV. With decreasing Z_{bound} the deduced excitation energies reach up to about two times the nuclear binding energy per nucleon.

In the upper part of figure 9 these energy deposits are compared to predictions of the Moscow statistical multifragmentation model [58]. In these calculations the model parameters have been adjusted [59] to describe the observed fragment yields (see for example center and lower parts of figure 9). For the

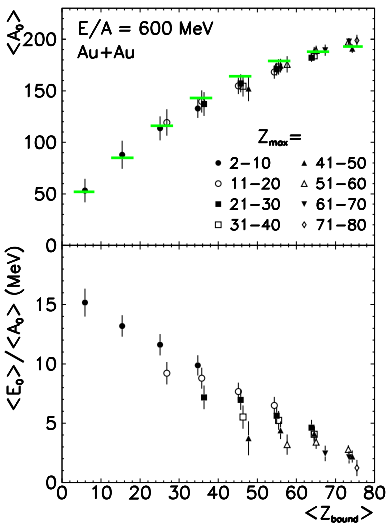

Figure 8: Average prefragment size $\langle A_0 \rangle$ and its excitation energy per nucleon $\langle E_0 \rangle / \langle A_0 \rangle$ as a function of Z_{bound} for different bins in Z_{max} [73]. The horizontal bars in the upper part mark the spectator size expected from a pure participant-spectator geometry.

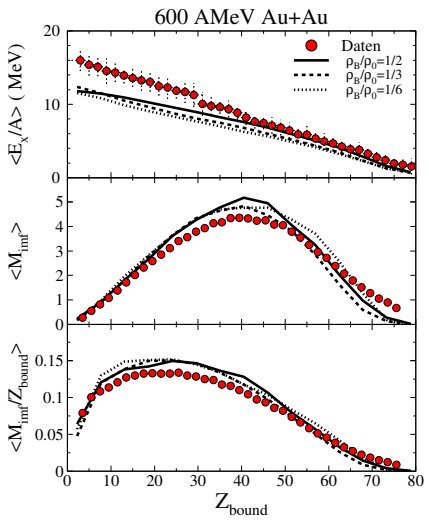

Figure 9: Excitation energy per nucleon (top part), mean IMF multiplicity (middle part) and normalized IMF multiplicity (lower part) as a function of Z_{bound}. The lines show results of the Moscow statistical multifragmentation model [58,59].

range of small Z_{bound} these two energies differ significantly. Potentially this difference signals the presence of (radial) collective motion at the time of breakup (see also refs. [60,34]).

3 Hadronic Thermometer

Less straightforward is the determination of a nuclear temperature. Nuclei are closed systems without an external heat bath. Consequently, the temperature of the system cannot be pre-determined but has to be reconstructed from observable quantities. For a microcanonical ensemble, the thermodynamic temperature of a system may be defined in terms of the total-energy state density. An experimental determination of the state density and its energy dependence is, however, hitherto impossible. Therefore, nuclear temperature determinations take recourse to 'simple' observables of specific degrees-of-freedom which constitute – at least for some ideal situations and generally within a canonical treatment – a good approximation to the true thermodynamic temperature.

Figure 10 illustrates three different methods to extract a temperature of

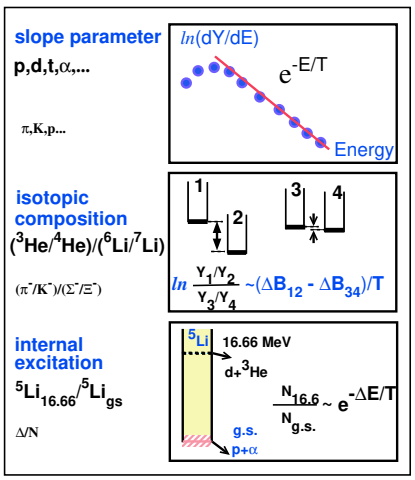

Figure 10: Illustration of different hadronic thermometer: inverse slope parameter (top part), isotope ratios (center part), and relative population of states (lower part).

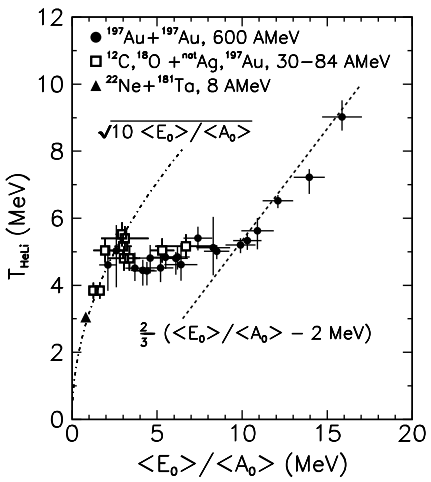

Figure 11: Caloric curve of nuclei determined by the dependence of the isotope temperature T_{HeLi} on the excitation energy per nucleon [73].

a hadronic system. At low excitation energies, the inverse slope parameters describing the kinetic energies or transverse mass distributions of the emitted particles are a good measure of the temperature. In relativistic nucleus-nucleus interactions, however, these distributions suffer from possible collective flow effects and secondary decay processes[61−64]. While the spectral distributions are indispensable to disentangle thermal and collective phenomena, a more direct way to test whether locally thermal equilibrium is achieved and to determine a temperature is to study in detail the particle abundance [65,66,67,68,69]. Finally, analysing the internal population of states of produced fragments, the so called emission temperature can be deduced. While the latter analysis requires a more demanding coincidence measurement of the decay products, isotope temperatures can be extracted from single particle yields.

For the following considerations we will assume a nuclear system at low density and in chemical and thermal equilibrium. For such a system a measure of the temperature T may be obtained via the double yield ratio of two isotope pairs, (Y_1/Y_2) and (Y_3/Y_4), differing by the same number of neutrons and/or protons [66]:

$$R = \frac{Y_1/Y_2}{Y_3/Y_4} = a \cdot e^{[(B_1-B_2)-(B_3-B_4)]/T}. \qquad (1)$$

Here, B_i denotes the binding energy of particle species i and the constant a contains known spins and mass numbers of the fragments. Of course, a meaningful temperature scale can only be derived if the ratio R is sufficiently sensitive to the temperature of the system and if the yields of the considered fragments are measurable over a large range of excitation energy. A large sensitivity of this thermometer can be achieved if the constant $b = (B_1 - B_2) - (B_3 - B_4)$ is larger than the typical temperature to be measured (see for example ref. [71] for details).

Particularly large values for b are obtained if a $^3He/^4He$ ratio is involved. Indeed, the large cross section of He fragments as an abundant constituent in both the 'liquid' and the 'vapor' regime of nuclear systems *and* the strong binding energy of the α-particle is the lucky coincidence which is the basis of the temperature determination presented hereafter. In order to acquire for the second yield ratio also a sufficient production yield we define in the following a temperature $T_{HeLi,0}$ in terms of the yield ratios ^{3}He/^{4}He and ^{6}Li/^{7}Li

$$T_{HeLi,0} := 13.33/ln(2.18 \cdot \frac{Y_{6Li}/Y_{7Li}}{Y_{3He}/Y_{4He}}). \qquad (2)$$

Using the d/t ratio rather than the ^{6}Li/^{7}Li ratio, a similar temperature scale, $T_{HHe,0}$, may be derived [66]. Whereas the d/t ratio was not accessible in the first experiment, $T_{HHe,0}$ may be more appropriate for central collisions. In general, by employing four nuclei species which all differ only little in proton and neutron numbers, emission from a similar stage of the reaction becomes more likely.

Up to this point we considered nuclei in their ground state only and we ignored the effect of sequential decays during the final stage of the disassembly process. In particular, the yield of α-particles may be modified by secondary decays. (Note, however, that the effect of the α-feeding is partially neutralized by the feeding of ^3He. Similarly, contributions from γ-unstable states in ^{6}Li and ^{7}Li partially cancel each other.) In order to test the model dependence of the temperature definition via Eq. (1) and to investigate the influence of sequential decays and low lying γ-unstable states we analyzed the fragment distributions predicted by several decay models [67,75,74,26]. Despite the strong feeding of the light particle yields through secondary decays these calculations predict an almost linear dependence of $T_{HeLi,0}$ on the actual temperature T of the system. However, in order to account pragmatically for a systematic

underestimation of the temperature by the quantity $T_{HeLi,0}$, we define the final isotope temperature via

$$T_{HeLi} = 1.2 \cdot T_{HeLi,0}. \tag{3}$$

For consistency reasons all values of T_{HeLi} presented hereafter include the factor 1.2. It is important to realize, though, that this calibration is model dependent and other decay models might predict different corrections (see for example [70,71]). Also each isotope thermometer will require an individual calibration [71,72]. This model dependence may only be reduced if more data on the population of excited states and the fragment distribution become available.

4 Nuclear Calorimetry

Figure 11 shows the isotope temperature as a function of the total excitation energy per nucleon[73]. This caloric curve can be divided into three distinctly different sections. In line with previous studies in the fusion evaporation regime[76] the rise of T_{HeLi} for excitation energies below 2 MeV per nucleon is compatible with the low-temperature approximation of a fermionic system. Within the range of $\langle E_0 \rangle / \langle A_0 \rangle$ from 3 MeV to 10 MeV an almost constant value for T_{HeLi} of about 4.5-5 MeV is observed. This plateau may be related to the finding of rather constant emission temperatures over a broad range of incident energies which were deduced from the population of particle unstable levels in He and Li fragments[77]. We also note that the mean excitation energy of the plateau coincides with the limiting excitation energy for the fusion-evaporation process of about 4.5-6.4 MeV per nucleon[78]. Finally, beyond a total excitation energy of 10 MeV per nucleon, a steady rise of T_{HeLi} with increasing $\langle E_0 \rangle / \langle A_0 \rangle$ is seen.

4.1 Caloric Curve of the Nuclear Fireball

While in central collisions between equally heavy nuclei the slope parameters and the collective radial motion are strongly interlaced, the chemical temperatures deduced from the isotopic composition reflect a local property and are expected to be less affected by a radial flow. Indeed, within the simple coalescence picture outlined in ref. [48] the double ratio entering into the evaluation of T_{HeLi} will be modified by not more than 5% for a typical ratio between flow and thermal energy of one.

The filled stars in Fig. 12 show values for T_{HeLi} for central Au+Au collisions at beam energies of 50, 100, 150 and 200 MeV per nucleon[80]. Central reactions were selected by the number of light particles detected in the forward

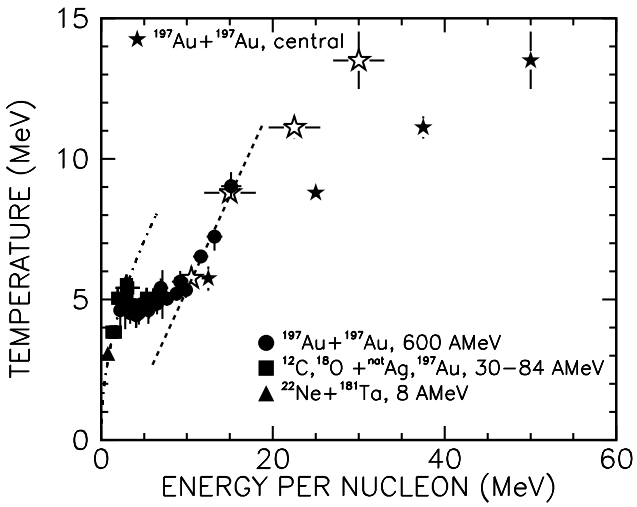

Figure 12: Caloric curve of nuclei determined by the dependence of the isotope temperature T_{HeLi} on the excitation energy per nucleon. The stars indicate results for central Au+Au collisions at 50, 100, 150 and 200 MeV per nucleon incident beam energy. For the filled stars the energy scale is given by the center-of-mass energy whereas in case of the open stars the radial flow energy (figure 5) has been subtracted. For orientation the lines given in Fig. 11 are also shown.

hemisphere in the center-of-mass[81]. Isotope ratios measured close to 90^o in the cm-system were used to evaluate the isotope temperatures[86]. For these data points, the *total* available center-of-mass energy per nucleon has been chosen as the horizontal axis. However, as discussed in chapter 2.1, only part of this energy is available for heating. For a proper comparison with the caloric curve determined by the spectator nuclei, one had to determine the thermal excitation energy *at normal density*. A lower limit for this energy can be obtained by subtracting the whole measured flow from the center-of-mass energy. The corresponding data points are indicated by the open stars in Fig. 12. Even considering the fact that the flow energy generated during the expansion from normal nuclear density towards the freeze-out density should be included in the energy scale, the similarity between the caloric curves in central and peripheral collisions is quite impressive and may be viewed as a signal of common underlying physics. Of course, a more quantitative understanding of the expansion dynamics will be required before the question can be answered whether and to what extent radial flow modifies the properties of the caloric curve.

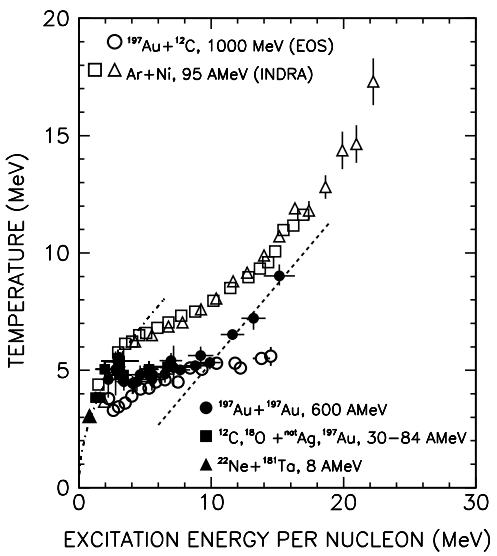

Figure 13: Comparison of ALADIN's caloric curve (solid points) to results obtained by the EOS collaboration for spectators produced in Au+C reactions at 1000 AMeV [82,83] (open circles) and by the INDRA collaboration for quasi-projectiles produced in 95 AMeV Ar+Ni reactions [84,85] (open triangles and squares).

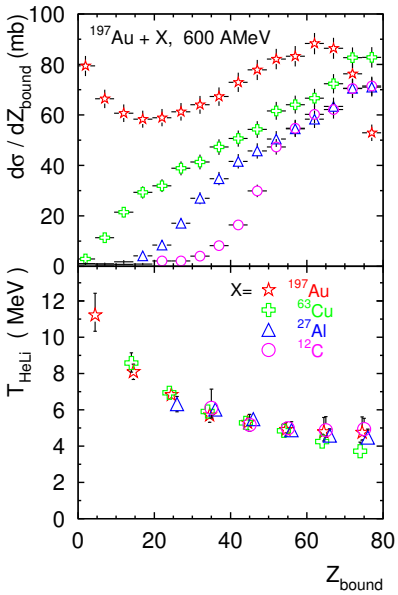

Figure 14: Lower part: Isotope temperatures as a function of Z_{bound} for Au+C,Al,Cu and Au reactions at 600 MeV per nucleon (from ref. [72]). Upper part: Differential cross section as a function of Z_{bound}.

4.2 Caloric Curves in other Reactions

The qualitative similarity of the caloric curve of water and that of nuclei is striking. Although it is clear, that *this analogy should not be overemphasized*, it was surely this resemblance which triggered a widespread activity, both experimental and theoretical. Figure 13 summarizes the presently available caloric curves measured via T_{HeLi} as defined in Eq. 3.

A recent result of the EOS collaboration for ^{197}Au+^{12}C reactions at 1000 AMeV beam energy is shown by the open circles [82,83]. These data nicely confirm the plateau-like behaviour at intermediate excitation energies between 5 and 10 MeV per nucleon, though the rise at high excitation energies is not observed in that experiment. This is in line with a similar observation by the ALADIN collaboration at 600 MeV per nucleon Au induced reactions on light targets [72] (lower part of Fig. 14). Though it is important to note that

for the light carbon target the cross section strongly drops for Z_{bound} values below about 40 (see circles in the upper part of Fig. 14). At small Z_{bound}, fluctuations in the decay as well as in the detection process might diminish the sensitivity of the event characterizing observable (here Z_{bound}) to the actual initial excitation energy for the central reactions in asymetric systems. As a consequence, no reliable temperature values can be extracted from the ALADIN data for Z_{bound} values less than 30. If also for the excitation energy the Z_{bound} universality holds this means that only the 'plateau' region can be probed by C+Au reactions.

The different reaction geometry represents a further possible source for the deviation between Au+Au and Au+C reactions: in Au+C reactions the participant and spectator regions have a larger overlap in momentum space. In addition, spectator nuclei produced in Au+Au reactions might be more compact compared to more rarified spectators in the most central Au+C collisions.

A *preliminary* result of the INDRA collaboration for the Ar+Ni system at E/A=95 MeV [84,85] is indicated by the open triangles and squares in Fig. 13. In this reaction, the half of the projectile-like source pointing into the beam direction has been analyzed. While the caloric curve of this quasi-projectile exhibits the qualitative behaviour of the ALADIN caloric curve, the temperature appears to be systematically higher by about 1-2 MeV. Clearly, more systematic studies are needed in order to clarify whether this discrepancy is for example due to the definition of the decaying source (which in the Fermi-energy regime is less clearly separated from the interaction region), the small size of the system in the Ar+Ni reaction (about 32 nucleons [84]) or the different neutron-to-proton contents of the source.

5 Emission Temperatures: The Breakdown of Equilibrium?

The validity of a hadronic thermometer generally rests on model assumptions. Only an experimental cross comparison with alternative thermometers can lend additional credibility to a temperature scale. For a cross calibration of the isotope thermometer with so called emission temperatures we, therefore, determined the relative population of excited states of light fragments in Au+Au reactions at various beam energies [80,86]. In figure 15 we compare the isotope temperature T_{HeLi} (closed symbols) with apparent emission temperatures deduced from the relative population of states in ^{5}Li (open symbols).

In central collisions at beam energies between 50 and 200 MeV we observe a clear discrepancy between the isotope temperature (closed crosses) and the emission temperature (open crosses) which is increasing with rising beam energy. (Note that the energy scale is not of prime relevance for this comparison.)

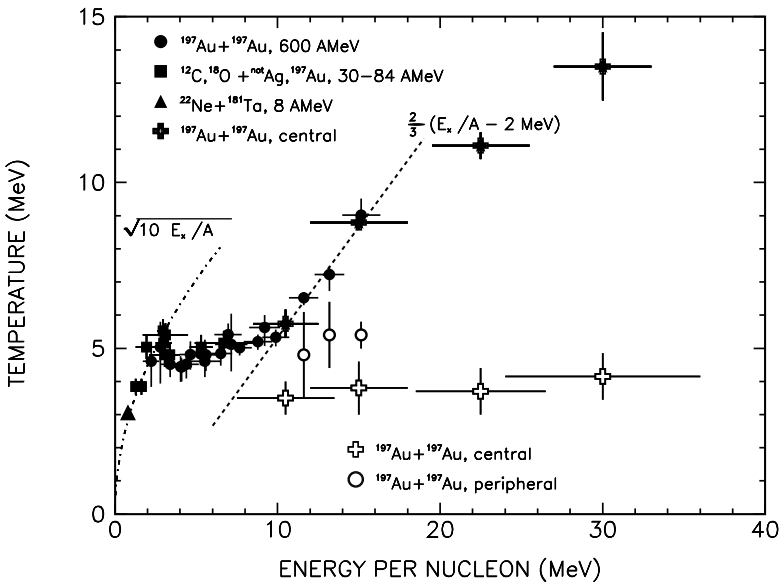

Figure 15: Comparison of the caloric curve measured via the isotope temperature T_{HeLi} (closed symbols) with apparent emission temperatures deduced from the relative population of states in ^{5}Li (open symbols; preliminary result from ref. [80]).

Besides the very low value of the emission temperatures of only 4 MeV, their constancy – despite an increase of the beam energy by a factor of four – is particularly striking. A similar divergence of the two thermometers is seen for the three uppermost central bins in spectator fragmentation at 600 resp. 1000 MeV per nucleon incident beam energy. Also there the emission temperatures (open circles) show a rather constant value, even though at a slightly higher level of about 5 MeV.

If the population of excited states is indeed as small and constant as the emission temperatures suggest, sequential decays will only moderately disturb the isotope temperatures and, moreover, the relative correction will not change significantly with increasing excitation or beam energy. Surely this corroborates the isotope ratios as a robust thermometer. But it also implies that - although sequential decays undoubtfully affects the difference between the emission and isotope temperatures – sequential feeding alone can probably not account for the observed discrepancy between the two thermometers [71].

Lacking at the moment a quantitative explanation of this surprising observation, it might be instructive to recall a similar phenomenon during the

cosmic big-bang. Also there different degrees-of-freedom freeze out at various stages of the big-bang evolution, hence signaling different temperatures. On first sight such a scenario appears to be rather disappointing since we would have to give up the idea of equilibrium between chemical and internal degrees of freedom at freeze-out. However, this complication may turn into an advantage in near future since the various thermometer might enable us to sample the thermodynamic evolution of the system.

6 Summary and Concluding Remarks

Disentangling collective and thermal motion in fireballs generated in central collisions, one observes a similar caloric behaviour as in spectator fragmentation at high excitation energies. This concordance suggests that, despite the very different underlying kinematics, the multifragment decays in both reaction types may be governed by common physics. Although various entrance channels lead to different caloric curves for quasi-projectiles, the qualitative agreement between these curves is encouraging. Clearly, a better knowledge of secondary processes and of the different experimental constraints is mandatory for a further interpretation of the observed differences.

The shape of the caloric curve as observed by the ALADIN collaboration is suggestive of a first-order phase transition with a substantial latent heat. It also seems to exclude - on first sight - the occurrence of a second-order phase transition which is the *sine qua non* for the determination of critical-point exponents [14,15]. For a finite system with N constituents a transition is, on the other hand, no longer characterized by a singular point but acquires a finite width over a temperature range ΔT_c around the transition temperature T_c. In case of a second order phase transition, $\Delta T_c/T_c$ is approximately given by $\Delta T_c/T_c \sim 1/\sqrt{N}$ [20]. For typical nuclear sizes of N$\approx$100, the influence of a second order phase transition may, therefore, be perceptible at temperatures deviating by as much as 10% from the critical value. Furthermore, for a classical van der Waals gas the latent heat increases close to the critical point with $\sqrt{1-T/T_c}$ and reaches already at $T/T_c = 0.95$ values larger than $k_B T_c$. Thus, in finite systems typical features of a first-order phase transition - like a latent heat - and signals indicating the proximity of the critical point - like diverging moments - are not necessarily inconsistent, making the attempt to extract critical-point exponents – at least – a worthwhile and interesting venture. Time must show, whether the hope to apply the concept of criticality to such small systems like nuclei is justified.

First hints (Fig. 9) and further experimental evidence[60] for the build-up of flow during a thermal driven decay of spectator nuclei have been found. This

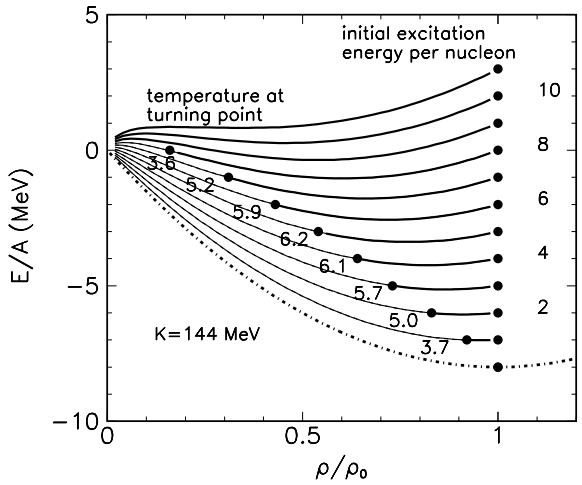

Figure 16: Evolution of an isentropically expanding Fermi gas in the energy per nucleon vs. density plane.

calls for a dynamical treatment of the fragmentation process. The dynamical evolution of the heated spectator nucleus will depend on its initial excitation energy and will, therefore, influence or even dominate the shape of the caloric curve. For illustration, the lines in Fig. 16 show the evolution of the summed thermal and potential energy for an isentropically expanding Fermi gas as a function of its density; the difference with respect to the initial energy at normal density (numbers on the right hand side) corresponds to the energy stored (momentarily) in the collective expansive motion. For the low density equation-of-state of the finite nuclear system, a parabolic density dependence

$$(E/A)_{T=0} = K_c/18 \cdot (1-\rho/\rho_0)^2 - 8MeV \qquad (4)$$

with a compressibility $K_c = 144$ MeV was used [32]. Furthermore, we ignore any dissipative processes during the expansion.

For initial excitation energies below about 8 MeV per nucleon the system is not able to expand freely to zero density but will stop at a finite density before it collapses again. Since at the turning point the Coulomb barrier reaches its minimum value and since the system spends most of its time in this region, it is probably reasonable to assume that the fragmentation happens at this point. Indeed, the temperatures at the turning point lie, rather independent

of the initial excitation energy, in the region of about 5 - 6 MeV. For excitation energies beyond 8 MeV per nucleon, the system may energetically expand to zero density prior to its freeze-out. In such a case, the initial energy would be subdivided in a potential energy of 8 MeV per nucleon and a collective flow energy. In our experiment, we do, however, observe high temperatures in the gas phase of the caloric curve. These high values signal a freeze out at a finite density, which is not too surprising considering the finite range of the strong interaction and considering the fact that the expansion velocity is still moderate. Within a more detailed calculation [33,34] the temperature of the 'gas branch' of the caloric curve can be explained with a nearly constant freeze-out density of about 1/3 of normal nuclear matter density.

While this interplay between the expansion dynamics and the density dependent properties of a Fermi gas might help to elucidate the gross features of the caloric curve one has to keep in mind that we are not dealing with a homogeneous system. An internally consistent equation-of-state taking into account the clusterisation [79], the particle loss during the expansion [31,33], the viscosity of nuclear matter, and the systematic variation of the source size in peripheral collisions as well as the explosive initial flow in central collisions [33] is required before more definite conclusions can be drawn. Nonetheless, if this scenario holds, the amount of radial motion which is transferred during the expansion into collective motion, will reflect both, the freeze-out density and the degree of dissipation during the expansion. Particle interferometry might provide another, independent, determination of the density of the system at freeze-out. Thus a combination of all these experimental informations might allow a closer look at the expansion dynamics.

Last but not least, a new, intriguing question resulted from the latest ALADIN experiment [86]: Why are the emission temperatures so low and – perhaps even more puzzling – why are they constant in central collisions despite a variation of the beam energy by a factor of four? While the associated small feeding contributions may be viewed as good news for the validity of the isotope thermometer, it clearly exemplifies that we are still far away from a detailed understanding of the thermodynamics of a finite, decaying nucleus.

All these open questions – and probably many more – will find their analogy in atomic cluster physics, cosmology and high energy particle/nuclear physics, where the concept of *phase-transition* is equally important. In this respect, a deeper understanding of the liquid-gas phase transition of nuclei might also shed some light on the past history of our universe as well as the world around us. Clearly, we could not provide an answer to the question raised in the beginning. All what we can definitely say is that nuclei do *not* behave just like ordinary water. Instead we are rewarded by the experience

of a rich variety of phenomena which originate – to a large extent though not exclusively – from the finite size of nuclei or, as expressed by Lucretius[2] when abandoning Empedocles' denial of void: *" nam corpora sunt et inane"*.

Acknowledgments

This work was supported in part by the European Community under contract ERBCHGE-CT92-0003 and ERBCIPD. J.P. and M.B. acknowledge the financial support of the Deutsche Forschungsgemeinschaft under the Contract No. Po256/2-1 and No. Be1634/1-1, respectively. We are especially grateful to W.G. Lynch, L.G. Moretto, J. Peter, E. Plagnol, and M.B. Tsang, for assistance in preparing this talk and for extensive discussions.

References

1. Empedocles, *fragment* 12/6 and 17/109 ($\approx$ 440BC), in Brad Inwood, *The Poem of Empedocles*, University of Toronto Press (1991).
2. Titus Lucretius Carus, *de rerum natura*, 1. book, verse 716*ff* (50BC).
3. N.K. Glendenning, *Phys. Rev.* C **46**, 1274 (1992).
4. R. Tamagaki, *Prog. Theor. Phys. Suppl. No.***112**, 1 (1993).
5. P.J. Siemens, NPA **428**, 189c (1984).
6. D.Q. Lamb *et al.*, *Phys. Rev. Lett.* **41**, 1623 (1978).
7. H. Jaqaman, A.Z. Mekjian, and L. Zamick, *Phys. Rev.* C **27**, 2782 (1983) and *Phys. Rev.* C **29**, 2067 (1984).
8. P.J. Siemens, *Nature* **305**, 410 (1983).
9. J.E. Finn *et al.*, *Phys. Rev. Lett.* **49**, 1321 (1982).
10. A.D. Panagiotou *et al.*, *Phys. Rev. Lett.* **52**, 496 (1984).
11. N.T. Porile *et al.*, *Phys. Rev.* C **39**, 1914 (1989).
12. X. Campi, *Phys. Lett.* B **208**, 351 (1988).
13. X. Campi, *J. Phys.*A **19**, L917 (1986).
14. M.L. Gilkes *et al.*, *Phys. Rev. Lett.* **73**, 1590 (1994).
15. J.B. Elliott *et al.*, *Phys. Rev.* C **49**, 3185 (1994).
16. W. Bauer and W.A. Friedman, *Phys. Rev. Lett.* **75**, 767 (1995) and M.L. Gilkes *et al.*, *Phys. Rev. Lett.* **75**, 768 (1995).
17. W. Bauer and A. Botvina, Phys. Rev. C **52**, R1760 (1995).
18. A. Hüller, these proceedings.
19. A. Wörner, *PhD thesis, Univ. Frankfurt* (1995) and W.F.J. Müller *et al.*, these proceedings.
20. Y. Imry, *Phys. Rev.* B **21**, 2042 (1980).
21. P. Labastie and R.L. Whetten, *Phys. Rev. Lett.* **65**, 1567 (1990).

22. D.H.E. Gross, L. Satpathy, Meng Ta-chung, and M. Satpathy, *Z. Phys.* A **309**, 41 (1982).
23. S. Levit and P. Bonche, *Nucl. Phys.* A **437**, 426 (1985).
24. L. Satpathy, M. Mishra, and R. Nayak, *Phys. Rev.* C **39**, 162 (1989).
25. J. Bondorf *et al.*, *Nucl. Phys.* A **444**, 460 (1985).
26. D.H.E. Gross, Zhang Xiao-ze, and Xu Shu-yan, *Phys. Rev. Lett.* **56**, 1544 (1986); D.H.E. Gross, *Prog. Part. Nucl. Phys.* **30**, 155 (1993).
27. L.G. Moretto *et al.*, *Phys. Rev. Lett.* **76**, 2822 (1996).
28. J. Pochodzalla *et al.*, *Phys. Rev. Lett.* **76**, 2823 (1996).
29. G. Bertsch and P.J. Siemens, *Phys. Lett.* B **126**, 9 (1983).
30. J.A. Lopez and P.J. Siemens, *Nucl. Phys.* A **431**, 728 (1984).
31. W.A. Friedman, *Phys. Rev.* C **42**, 667 (1990).
32. W.A. Friedman, *8-th Winter Workshop on Nuclear Dynamics, Jackson Hole, Wyoming, 1992.*
33. G. Papp and W. Nörenberg, *International Workshop XXII on Gross Properties of Nuclei and Nuclear Excitations*, Hirschegg 1994, p. 87.
34. G. Papp, these proceedings.
35. P.A. Hervieux and D.H.E. Gross, *Z. Phys.* D **33**, 295 (1995); D.H.E. Gross and P.A. Hervieux, *Z. Phys.* D , (in print).
36. D.J. Wales and I. Ohmine, *J. Chem. Phys.* **98**, 7245 (1993).
37. H.-P. Cheng *et al.*, *Phys. Rev.* A **46**, 791 (1992).
38. A. Hüller, *Z. Phys.* B **93**, 401 (1994).
39. R. Blümel *et al.*, *Nature* **334**, 309 (1988).
40. M.B. Tsang *et al.*, *Phys. Rev. Lett.* **71**, 1502 (1993).
41. S.C. Jeong *et al.*, Phys. Rev. Lett. **72**, 3468 (1994).
42. W.C. Hsi *et al.*, *Phys. Rev. Lett.* **73**, 3367 (1994).
43. W. Bauer *et al.*, *Phys. Rev.* C **47**, R1383 (1993).
44. W. Reisdorf *et al.*, in *International Workshop XXII on Gross Properties of Nuclei and Nuclear Excitations, Hirschegg, 1994*, p. 93.
45. D. Heuer *et al.*, *Phys. Rev.* C **50**, 1943 (1994).
46. M.A. Lisa *et al.*, *Phys. Rev. Lett.* **75**, 2662 (1995).
47. R. Pak *et al.*, *Michigan State University pre-print, MSUCL-1017* (1996).
48. G.J. Kunde *et al.*, *Phys. Rev. Lett.* **74**, 38 (1995).
49. J. Bondorf *et al.*, *Phys. Rev. Lett.* **73**, 628 (1994).
50. J. Hubele *et al.*, *Z. Phys.* A **340**, 263 (1991); *Phys. Rev.* C **46**, R1577 (1992).
51. P. Kreutz *et al.*, *Nucl. Phys.* A **556**, 672 (1993).
52. C.A. Ogilvie *et al.*, *Phys. Rev. Lett.* **67**, 1214 (1991).
53. A. Schüttauf, *PhD-thesis, University Frankfurt* (1996) and A. Schüttauf *et al.*, GSI-preprint 96-26 (1996) and nucl-ex/9606001.

54. L. Beaulieu *et al.*, Chalk River Laboratories pre-print TASCC-P-96-12 (1996).
55. V. Lips *et al.*, *Phys. Rev. Lett.* **72**, 1604 (1994).
56. G.F. Peaslee *et al.*, *Phys. Rev.* C **49**, R2271 (1994).
57. X. Campi, H. Krivine, and E. Plagnol, *Phys. Rev.* C **50**, R2680 (1994).
58. A.S. Botvina *et al.*, *Nucl. Phys.* A **584**, 737 (1995).
59. W.D. Kunze, *PhD-thesis University Frankfurt* (1996).
60. R. Lacey *et al.*, these proceedings.
61. R. Brockmann *et al.*, *Phys. Rev. Lett.* **53**, 2012 (1984).
62. S.A. Bass *et al.*, *Phys. Lett.* B **335**, 289 (1994).
63. Ch. Müntz *et al.*, *Z. Phys.* A **352**, 175 (1995).
64. J. Pochodzalla *et al.*, *Phys. Rev.* C **35**, 1695 (1987).
65. F. Hoyle, *Monthly Notices of the Royal Astronom. Soc.* **106**, 343 (1946).
66. S. Albergo *et al.*, *Nuovo Cimento A* **89**, 1 (1985).
67. D. Hahn and H. Stöcker, *Nucl. Phys.* A **476**, 718 (1988).
68. P. Braun-Munzinger *et al.*, *Phys. Lett.* B **344**, 43 (1995) and *Phys. Lett.* B **365**, 1 (1996).
69. A.D. Panagiotou *et al.*, *Phys. Rev.* C **53**, 1353 (1996).
70. J. Pochodzalla *et al.*, *Phys. Rev. Lett.* **55**, 177 (1985).
71. M.B. Tsang *et al.*, these proceedings.
72. T. Möhlenkamp, *PhD-thesis, University Dresden* (1996).
73. J. Pochodzalla *et al.*, *Phys. Rev. Lett.* **75**, 1040 (1995).
74. R.J. Charity *et al.*, *Nucl. Phys.* A **483**, 371 (1988).
75. J. Konopka *et al.*, *Phys. Rev.* C **50**, 2085 (1994).
76. D. Fabris *et al.*, *Phys. Lett.* B **196**, 429 (1987) and references therein.
77. G.J. Kunde *et al.*, *Phys. Lett.* B **272**, 202 (1991).
78. W. Bohne *et al.*, *Phys. Rev.* C **41**, R5 (1990).
79. G. Peilert *et al.*, *Phys. Lett.* B **260**, 271 (1991).
80. V. Serfling, *PhD-thesis, University Frankfurt* (1996) and to be published.
81. Except for the trigger condition (at least two particles in the hodoscope [86]) no additional centrality cut was applied at E/A=50 MeV in the present stage of the analysis.
82. M.L. Tincknell *et al.*, *Proceedings of the 12th Winter Workshop on Nuclear Dynamics* (1996).
83. J.A. Hauger *et al.*, these proceedings.
84. J. Peter (INDRA collaboration), private communication.
85. G. Auger *et al.*, these proceedings.
86. G. Immé *et al.*, these proceedings.